Why nitrogen oxide inhibits CO oxidation over highly dispersed platinum ceria catalysts

Catalysis Today 426 (2024) 114394

Contents lists available at ScienceDirect

Catalysis Today

journal homepage: www.elsevier.com/locate/cattod

Why nitrogen oxide inhibits CO oxidation over highly dispersed platinum ceria catalysts

Mengqiao Di [a,1], Andreas Schaefer [a,2], Felix Hemmingsson [a,3], Tamsin Bell [b], Yanyue Feng [a,4], Magnus Skoglundh [a,5], David Thompsett [b,6], Per-Anders Carlsson [a,*,7]

[a] Competence Centre for Catalysis, Department of Chemistry and Chemical Engineering, Chalmers University of Technology, Gothenburg 412 96, Sweden
[b] Johnson Matthey Technology Centre, Blounts Court, Sonning Common, Reading RG4 9NH, UK

ARTICLE INFO

Keywords:
Low-temperature activity
Supported catalyst
Interfacial reactions
Mars-van Krevlen
Infrared spectroscopy
DRIFTS

ABSTRACT

The influence of nitrogen oxide on the lean CO oxidation activity of highly dispersed Pt/ceria and reference Pt/alumina catalysts has been studied by kinetic measurements and infrared spectroscopic characterization. Co-feeding of nitrogen oxide leads to the formation of nitrates on the supports that induce a highly oxidized character of the Pt sites and in the case of Pt/ceria, inhibit ceria lattice oxygens to react with CO adsorbed on Pt rim sites via a Mars-van Krevelen mechanism below the ignition temperature. The build-up of nitrates below the light-off temperatures is faster when CO is present in the feed. Above the light-off temperatures, carbonates replace the nitrates while the catalytic activity remains high.

1. Introduction

The catalytic removal of carbon monoxide (CO) from process and exhaust streams is much dependent on other compounds present in the stream. These compounds do not have to be serious catalyst poisons such as sulfur and phosphorus oxides, but can be molecules that interact more weakly with the catalyst, still affecting essential catalyst functions. A clear example is the aftertreatment of combustion gases where air is used as the main source of oxidant in the combustion. This leads to the formation of nitrogen oxides (NO_x), which not only pose a pollution problem in itself but also complicates the catalytic abatement of CO emissions.

Supported platinum catalysts are among the most robust catalysts for CO oxidation. Highly active catalysts can be designed by supporting platinum onto ceria [1,2]. In a previous study, we investigated in detail the oxidation of CO over highly dispersed Pt/ceria and Pt/alumina catalysts synthesised by industrially relevant methods [3]. The as-prepared Pt/ceria and Pt/alumina catalysts exposed a total surface area of 140 and 131 m^2/g_{cat} and contained Pt particles with an average size of 1.5 and 2 nm, respectively. From *operando* infrared spectroscopic measurements it was concluded that for Pt/ceria, spectator CO ad-species on ionic platinum exist even at high temperatures with high CO conversions while the CO oxidation proceeds on sites on the Pt particles. *Operando* X-ray absorption spectroscopic measurements reveal that these particles exhibit a high oxidation state and Pt-O coordination is dominating. During the protracted catalytic extinction, the CO coverage builds up gradually while the Pt oxidation state and Pt-O coordination remain high due to the interactions with the ceria support. The observed CO oxidation at low temperatures, i.e., at high CO coverages, proceeds on sites at the platinum-ceria boundary that cannot be CO self-poisoned (both CO and O_2 reaction orders are close to zero), following a Mars-van Krevelen mechanism involving ceria lattice oxygens that react with CO adsorbed on platinum rim sites [4]. This behavior is in stark contrast to that of the reference Pt/alumina catalyst,

* Corresponding author.
E-mail address: per-anders.carlsson@chalmers.se (P.-A. Carlsson).
[1] 0000-0002-9271-4929
[2] 0000-0001-6578-5046
[3] 0000-0002-3773-373x
[4] 0000-0003-0838-3539
[5] 0000-0001-7946-7137
[6] 0000-0002-1223-5910
[7] 0000-0001-6318-7966

https://doi.org/10.1016/j.cattod.2023.114394
Received 19 June 2023; Received in revised form 14 September 2023; Accepted 23 September 2023
Available online 28 September 2023

which shows a clear removal of platinum oxides formed during CO oxidation and the classical drop in catalytic activity caused by rapid CO self-poisoning when reaching a critical temperature.

The present aim is to explore the effect of NO on the activity for CO oxidation over these catalysts, and to give a rather detailed infrared spectroscopic analysis of the surface species under reaction conditions to explain this effect.

2. Experimental

2.1. Basic characterisation of spent catalysts

The catalyst preparation and basic characterisation of as-prepared Pt/ceria and reference Pt/γ-alumina catalysts were described briefly in the Introduction and the detailed descriptions can be found in previous work [3]. Here some additional characterisation of the spent catalysts, i.e., after being used for CO oxidation in presence of NO is done.

The crystalline phases of the spent catalysts were analysed by powder X-ray diffraction (PXRD) using a D8 Discover diffractometer (Bruker) equipped with a Cu-K_α X-ray source (1.5418 Å) and a EIGER2 R 500 K Hybrid Photon Counting (HPC) detector. Diffracted X-rays were recorded under ambient conditions with a variable slit and a fixed sample illumination of 7 mm in the 2θ range from 20 to 91° with an incremental step of 0.02°. Each step was measured for 2 s.

The spent catalysts were also imaged by high-resolution transmission electron microscopy (HRTEM) and scanning transmission electron microscopy (STEM) using a Tecnai T20 microscope (FEI) and a Titan 80–300 microscope (FEI), respectively. The Tecnai T20 microscope was equipped with a LaB_6 filament operated at 200 kV and a high-angle annular dark-field STEM detector. A field emission gun operated at 300 kV was used for the Titan 80–300 microscope. The specimen was prepared by dispersing the catalyst in ethanol using ultrasonication for enhanced mixing. A droplet of the obtained suspension was then applied to a holey carbon film supported on a copper grid. The recorded micrographs were analysed using ImageJ [5] as to extract Pt particle size distributions.

2.2. Catalytic tests

The catalytic performance was evaluated using a stainless steel fixed-bed powder reactor, as described in detail elsewhere [6], positioned in a vertical flow direction. In brief, the sample was placed in the 4 mm wide and 16 mm long sample compartment, and a type K thermocouple was located 2 mm into the sample bed. The reactor was heated resistively by an inbuilt heating coil using a PID regulator and another type K thermocouple for measuring the reactor block temperature. The entire reactor was insulated. The feed gas composition was composed by a set of mass flow controllers (Bronkhorst). The effluent gas was analysed by mass spectrometry (Pfeiffer Vacuum GSD-350) following the *m/e* ratios: 2 (H_2), 18 (H_2O), 28 (CO), 32 (O_2) and 44 (CO_2).

The powder samples were sieved and the fraction between 100 and 300 μm was kept and diluted with ground cordierite sieved to the same fraction. Around 10 mg of catalyst was mixed with 90 mg ground cordierite, and then loaded into the reactor. Catalytic tests were carried out using 0.2 vol% CO, 1 vol% O_2 and 300 ppm of NO. The total flow was 150 ml/min and constant, and Ar was used as carrier gas throughout the measurements. The reactor temperature was first increased from room temperature to 350 °C with a rate of 5 °C/min and dwelled for one hour in the reaction mixture. Then a catalytic extinction-ignition cycle was repeated three times by cooling the reactor to 35 °C, dwell for 10 min and then increasing the temperature again to 350 °C and dwelling for 30 min before repeating the next two extinction-ignition cycles. Additional catalytic tests in which the catalyst has been pre-exposed to nitrogen oxide (300 ppm NO, 2 h, 35 °C) were also carried out. The catalytic ignition was studied by increasing the reactor temperature to 350 °C with a rate of 5 °C/min after purging with Ar for 20 min

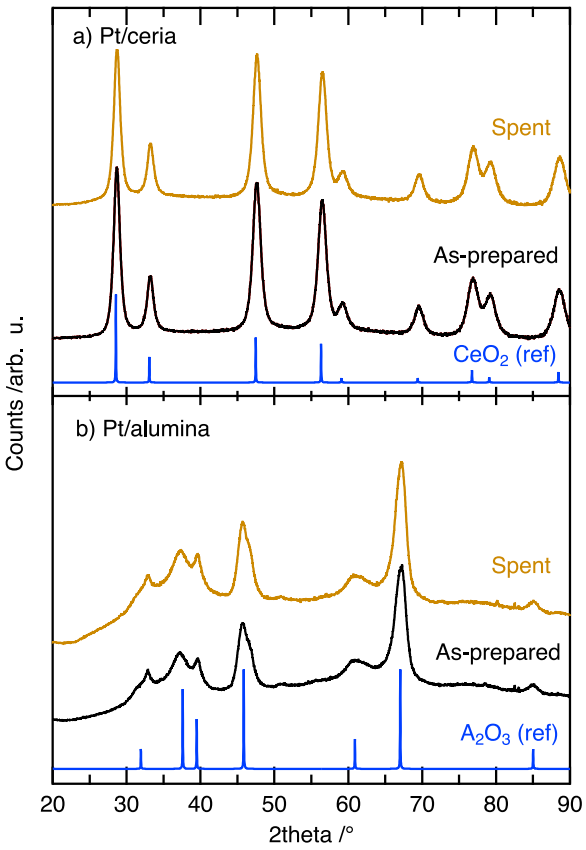

Fig. 1. XRD patterns of the a) spent Pt/ceria in and b) spent Pt/alumina sample, i.e., after CO oxidation with NO (brown), and as-prepared Pt/ceria and as-prepared Pt/alumina samples (black). Reflection assignments are assigned using reference patterns (blue) from the Powder Diffraction File™ (PDF) database for CeO_2 (PDF 00–004–0593) and γ-Al_2O_3 (PDF 00–010–0425).

2.3. Infrared spectroscopic characterization

Infrared spectroscopic speciation of adsorbates was done in diffuse reflectance mode (DRIFTS) using a VERTEX 70 spectrometer (Bruker) set-up as described elsewhere [3]. A high-temperature stainless steel reaction chamber (Harrick Inc.) with CaF_2 windows was mounted inside a Praying Mantis mirror accessory (Harrick Inc.). One type K thermocouple was inserted into the sample holder to measure the catalyst bed temperature in the IR probing volume and another thermocouple was placed underneath the sample holder for control of the reactor heating. The feed gas was composed by individual mass flow controllers (Bronkhorst) mixing suitable flows of 10 %CO, 100 % O_2 and 3 % NO in Ar with pure Ar to the desired feed composition.

The measurements were carried out using either 55 mg Pt/ceria or 45 mg of the Pt/alumina catalyst in the sample holder. First the catalyst was pretreated with 5 vol% O_2 for 40 min, then 2 vol% H_2 for 30 min followed by pure Ar flow for 2 h at around 200 °C (measured temperature underneath the DRIFTS cell was 211 °C), to establish steady levels of the mass spectrometer signals. The total gas flow was kept constant at 100 ml/min. Then, the temperature was decreased in steps to 35 °C and a background spectrum was recorded in the range 400–4400 cm^{-1} with a resolution of 1 cm^{-1} at each temperature. The background spectra were recorded by averaging 100 scans using a 6 mm aperture and 20 kHz scanner velocity. After this, the feed mixture containing 0.2 vol% CO, 2 vol% O_2 and 300 ppm NO was introduced and fed for 4 h at 35 °C while recording a spectrum every ten minutes averaging over 50 scans. Thereafter, a CO ignition/extinction experiment was carried out by increasing/decreasing the temperature in steps. A spectrum was collected after 10 min at each temperature. Also, CO ignition

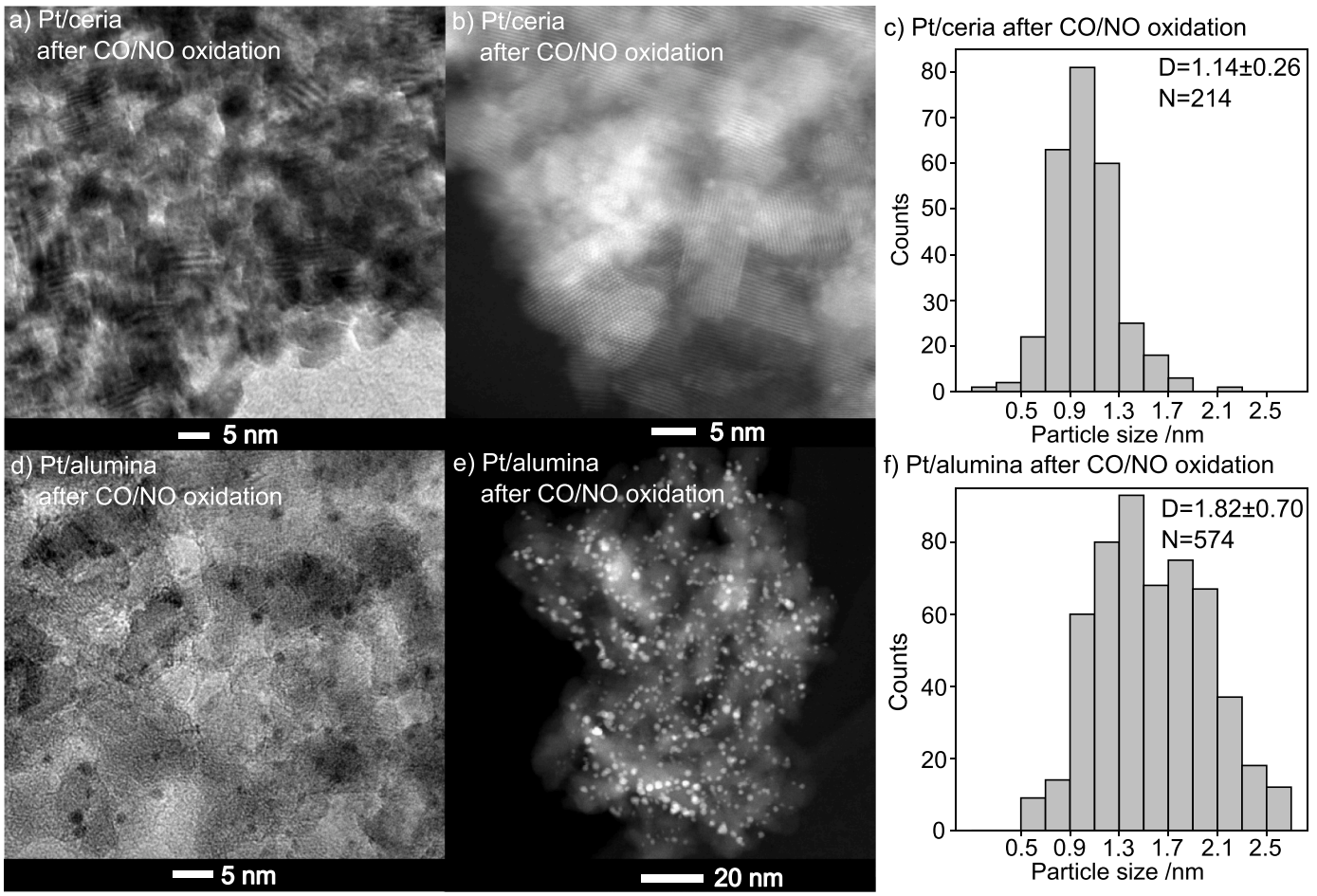

Fig. 2. High-resolution TEM and STEM-HAADF micrographs of the spent Pt/ceria (panel a,b) and spent Pt/alumina (panel d,e) catalysts after CO oxidation in presence of NO. The average Pt particle size for the spent Pt/ceria (panel c) is 1.14 nm based on 214 Pt particles, and for the spent Pt/alumina (panel f) 1.82 nm based on 574 Pt particles.

measurements in which the pretreatment procedure included a final step of exposing the sample to 300 ppm NO at 35 °C for 2 h were carried out. Subsequently, CO oxidation was carried by stepping up the temperature as above while collecting spectra at each temperature. Further, measurements where the pretreatment was finished with 0.2 vol% CO for 2 h at 35 °C followed by exposing the sample to 300 ppm NO keeping the temperature constant while recording spectra every 10 min for 4 h were carried out.

3. Results and discussion

We start off this section by commenting on the physical characteristics of the catalysts. Then follows a discussion of the catalytic performance tests and the infrared characterisation.

3.1. X-ray diffraction and electron microscopy analyses

Fig. 1 shows the X-ray diffractograms of the spent catalysts after CO oxidation in presence of NO for Pt/ceria (panel a) and Pt/alumina (panel b). Diffractograms for the as-prepared catalysts are included for comparison and the patterns for γ-alumina (PDF 00-010-0425) and CeO_2 fluorite structure (PDF 00-004-0593) are included as references. The diffractograms of the spent catalysts are identical to the corresponding ones of the as-prepared catalysts. Further, the diffractogram of the Pt/ceria and Pt/alumina sample matches the reference pattern of fluorite CeO_2 and γ-alumina, respectively. The apparent support crystallite size was calculated by use of the Sherrer equation. The ceria crystallite size is found to be 7 nm for both the as-prepared and spent catalysts. Likewise, the alumina crystallite size for the as-prepared and spent Pt/alumina samples is found to be 7 nm. The diffractograms present no observable peaks for Pt phases. The support crystallite sizes can also be estimated from the TEM images shown in the left column of Fig. 2 (panels a and d). Here, the size of the ceria and alumina crystallites is around 7 and 10 nm, respectively.

Concerning the Pt phase, TEM imaging is for these samples superior to standard PXRD for analysis of the presence of small Pt particles. In addition to TEM images, Fig. 2 displays STEM images (panels b and e) and estimated particle size distributions (PSD) for the two catalysts after being exposed to CO oxidation reaction conditions including NO. For the spent Pt/ceria sample, the Pt particles appear somewhat diffuse in the TEM images in part due to the small difference in mass between Pt and Ce, and in part, because low mass-thickness contrast originating from thickness variations in the specimen. Nevertheless, the observed fringes are indicative of a superposition of different types of crystal planes, which orient in different directions. In the STEM images, however, the Pt particles can be clearly distinguished from the ceria support thanks to the difference in atomic number. The PSDs for the spent catalysts are nearly unaltered due to exposure to CO oxidation reaction conditions with NO co-feeding. For Pt/ceria, the majority of the Pt particles in the size-range of 0.7–1.7 nm whereas for the spent Pt/alumina sample, the majority of the Pt particles falls within the range of 0.7–2.5 nm.

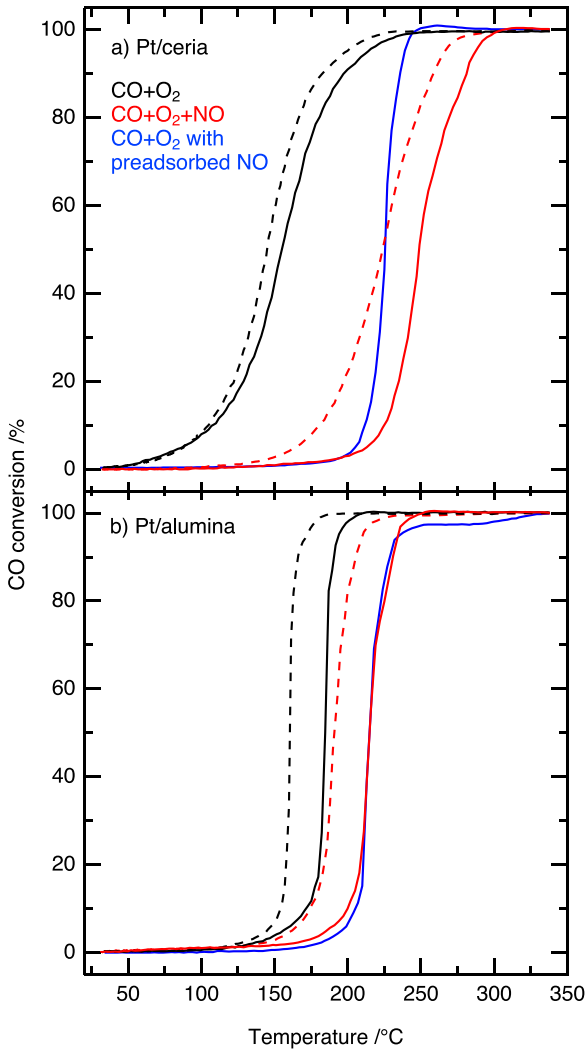

Fig. 3. CO conversion as a function of inlet gas temperature during ignition (solid lines) and extinction (dashed lines) for a) Pt/alumina and b) Pt/ceria when exposed to either 0.2 vol% CO and 1 vol% O_2 (black), 0.2 vol% CO, 1 vol % O_2 and 300 ppm NO (red) or 0.2 vol% CO and 1 vol% O_2 after preadsorption of NO (blue).

3.2. Flow-reactor results

The measured CO conversions over the Pt/ceria and Pt/alumina catalysts during catalytic ignition and extinction (third cycle) w/wo NO present in the feed as well as during ignition with preadsorbed NO are shown in Fig. 3. The CO conversion changes rapidly from high-to-low in a narrow temperature interval when the temperature is increased, or vice versa, reflecting the typical kinetic behaviour of CO oxidation [3, 7–10]. Principally, the hysteresis is widened by heat and mass transfer characteristics, i.e., transport of heat generated by the exothermic oxidation reactions and mass transfer rates of the limiting reactant CO. Here, the adiabatic temperature difference due to CO oxidation is about 20 °C, but the rigorous dilution with inert material lowered the practical temperature increase to 4 °C as measured by the thermocouple positioned in the rear catalytic bed. Thus thermal effects are small.

For both catalysts, it is clear that the CO conversion profiles generally shift towards higher temperatures when NO is present in the feed or pre-adsorbed on the samples.

In more detail, the light-off temperature, here denoted with T_{50}^{ig} signifying 50 % CO conversion during ignition, increases from 155 to 248 °C for the Pt/ceria catalyst whereas for the extinction process, the corresponding T_{50}^{ex} increases from 145 to 224 °C. The width of the ignition-extinction hysteresis, i.e., here defined as the temperature difference T_{50}^{ig} - T_{50}^{ex}, changes from 10 °C for pure CO oxidation to 24 °C when NO is present. When NO is pre-adsorbed, the start of the CO conversion is shifted similarly to the case with NO co-feeding. Upon ignition, however, the CO conversion increases more rapidly and the T_{50}^{ig} is lower, 226 °C, as compared to the case of continuous NO supply. For the Pt/alumina catalyst, the CO conversion profiles during catalytic ignition/extinction measurements exhibit rapid changes in the CO conversion at low temperatures. The light-off temperature increases from 185 °C to 215 °C when NO is co-fed. Similarly the T_{50}^{ex} increases from 161 °C to 191 °C when NO is added to the feed. The width of the hysteresis, here defined as the temperature difference T_{50}^{ig} - T_{50}^{ex}, is the same (24 °C) w/wo NO present. For the ignition with pre-adsorbed NO, T_{50}^{ig}, the conversion profile is nearly the same as in the case of co-feeding of NO. Clearly NO inhibits the CO oxidation for both catalysts. For Pt/ceria, the CO conversion curves in presence of NO are similar to the curves for Pt/alumina, indicating that the Mars-van Krevelen mechanism involving ceria lattice oxygen is blocked.

3.3. In situ infrared spectroscopy

To shine some light on the NO inhibition, in situ infrared spectroscopy was used to monitor surface species during CO oxidation in the presence of NO while increasing/decreasing the temperature in steps in the temperature region spanned in the flow-reactor ignition/extinction measurements. Also a few complementary time-resolved measurements at constant temperature are included as to strengthen the analysis. The general assignment of infrared absorption bands to, e.g., -CO, -OH and -NO surface species, can often be done without major uncertainties, but the more specific assignments to adsorbates occupy particular sites and interact with each other are many times open for debate even when supported with theoretical calculations. Here, the peaks stemming from Pt bound species are rather safely assigned whereas peaks arising from species bound to the supports are not always straightforward to interpret. In this section, the IR spectroscopic results will be presented and discussed aiming at a qualitative understanding of the NO inhibition effect. A summary of IR peak assignments for ceria and alumina bound species is given in Table 1 whereas those for platinum bound species are referenced continuously.

In Fig. 4 the infrared difference spectra collected for the Pt/ceria catalysts while increasing (panel a) and decreasing (panel b) the sample temperature in steps in the presence of 0.2 vol% CO, 1 vol% O_2 and 300 ppm NO in Ar are shown. The double IR band at around 2350 cm^{-1} signifies product CO_2 in the gas phase. It is denoted with $\tilde{\nu}_{gas}^{CO_2}$, which is one of the notation styles to be used for identified species hereafter. Starting off with the ignition over the Pt/ceria catalyst, the $\tilde{\nu}_{gas}^{CO_2}$ band becomes visible at 52 °C and increases in intensity with increased temperature reflecting increased CO conversion to CO_2. The peak at 2230 cm^{-1} is assigned to isocyanate species linearly bound to ceria ($\tilde{\nu}_{lin}^{NCO}$(ceria)). Adsorbed N_2O also gives rise to a peak at this position, however, it adsorbs weakly and is expected to exist only at low temperatures [11]. Here, the peak is visible also at higher temperatures and it is thus more likely to originate from isocyanate species. The intensity of the $\tilde{\nu}_{lin}^{NCO}$(ceria) band increases with increased temperature until 130 °C is reached above which it decreases upon further increase of the temperature. The peaks at 1930, 1750, and 1675 cm^{-1} are assigned to species bound to Pt. The bands at 1750 and 1674 cm^{-1} are assigned to NO bonded to Pt in linear ($\tilde{\nu}_{lin}^{NO}(Pt^0)$) and bridged ($\tilde{\nu}_{br}^{NO}(Pt^0)$) configuration, respectively [12]. The minor peak at 1930 cm^{-1} could either be assigned to CO adsorbed on platinum-ceria boundary sites ($\tilde{\nu}_{lin}^{CO}(Pt\text{-}Ce^{3+})$) or NO adsorbed on oxidic platinum ($\tilde{\nu}_{lin}^{NO}(Pt^{2+})$) [13,14]. With increasing temperature, the $\tilde{\nu}_{lin}^{NO}(Pt^0)$ and $\tilde{\nu}_{br}^{NO}(Pt^0)$ disappear whereas the intensity

Table 1
Assignment of identified IR bands corresponding to species adsorbed on the supports for the Pt/ceria and Pt/alumina catalysts.

Wavenumber /cm^{-1}		Assignment	Notation	Vibration	Reference
1587, 1297, 1010	Ceria	Bidentate carbonate	b-CO_3	$\tilde{\nu}_{as}(CO_3^{2-})$ splitting, $\tilde{\nu}_{s}(CO_3^{2-})$	[15]
1738, 1402, 1220		Bridged carbonate	br-CO_3	$\tilde{\nu}_{as}(CO_3^{2-})$ splitting, $\tilde{\nu}_{s}(CO_3^{2-})$	[16]
1606, 1393, 1037		Bridged hydrogen carbonate	br-(CO_2)OH	$\tilde{\nu}_{as}(CO_3^{2-})$ splitting, $\tilde{\nu}_{s}(CO_3^{2-})$	[17,18]
3617, 1218				$\tilde{\nu}$(OH), δ(OH)	[17,18]
1490, 1371		Monodentate carbonate	m-CO_3	$\tilde{\nu}_{as}(CO_3^{2-})$ splitting	[17,18]
1475, 1033		Polydentate carbonate	p-CO_3	$\tilde{\nu}$(C = O)	[15]
1460, 1357				$\tilde{\nu}_{as}(CO_3^{2-})$ splitting	[15]
1581, 1240, 1033		Bidentate nitrate	b-NO_3	$\tilde{\nu}_{as}(NO_3^{2-})$ splitting, $\tilde{\nu}_{s}(NO_3^{2-})$	[19,20]
1591, 1212, 1010		Bridged nitrate	br-NO_3	$\tilde{\nu}_{as}(NO_3^{2-})$ splitting, $\tilde{\nu}_{s}(NO_3^{2-})$	[19,20]
1551, 1276, 1010		Monodentate nitrate	m-NO_3	$\tilde{\nu}_{as}(NO_3^{2-})$ splitting, $\tilde{\nu}_{s}(NO_3^{2-})$	[19,20]
1475, 1033		Monodentate nitrite	m-NO_2	$\tilde{\nu}$(N = N), $\tilde{\nu}$(NO)	[21]
1433, 1322		Polydentate nitrate	p-NO_3	$\tilde{\nu}_{as}(NO_3^{2-})$ splitting	[20–22]
1433, 1322		Water-solvated nitrate	NO_3(OH)	$\tilde{\nu}_{as}(NO_3^{2-})$ splitting	
		Nitro compound	NO_2	$\tilde{\nu}_{as}$(NO), $\tilde{\nu}_{s}$(NO)	
		trans-hyponitrite	*trans*-$N_2O_2^{2-}$	$\tilde{\nu}$(N = N)	
1361, 1058		*cis*-hyponitrite	*cis*-$N_2O_2^{2-}$	$\tilde{\nu}$(N = N), $\tilde{\nu}$(NO)	[22,23]
1605, 1322		Weakly adsorbed NO_2	NO_2	$\tilde{\nu}_{as}$(NO), $\tilde{\nu}_{s}$(NO)	[22]
1186		Nitrosyl anion	NO^-	$\tilde{\nu}$(NO)	[23,24]
1544, 1255	Alumina	Bidentate carbonate	b-CO_3	$\tilde{\nu}_{as}(CO_3^{2-})$ splitting	[25]
1655, 1228, 1429		Bridged carbonate	br-CO_3	$\tilde{\nu}_{as}(CO_3^{2-})$ splitting, $\tilde{\nu}_{s}(CO_3^{2-})$	[26]
		Bridged hydrogen carbonate	br-(CO_2)OH)	$\tilde{\nu}$(CO),δ(COH), $\tilde{\nu}_{s}(CO_3^{2-})$	
1459, 1352		Polydentate carbonate	p-CO_3	$\tilde{\nu}_{as}(CO_3^{2-})$ splitting	[25]
1596, 1308		Bidentate nitrate	b-NO_3	$\tilde{\nu}_{as}(NO_3^{2-})$ splitting	[26,27]
1618, 1274		Bridged nitrate	br-NO_3	$\tilde{\nu}_{as}(NO_3^{2-})$ splitting	[26,27]
1553, 1308		Monodentate nitrate	m-NO_3	$\tilde{\nu}_{as}(NO_3^{2-})$ splitting	[26,27]
1487		Monodentate nitrite	m-NO_2	$\tilde{\nu}$(N = N)	[26,27]
1416, 1344		Polydentate nitrate	p-NO_3	$\tilde{\nu}_{as}(NO_3^{2-})$ splitting	[20,28]
		Water-solvated nitrate	NO_3(OH)	$\tilde{\nu}_{as}(NO_3^{2-})$ splitting	
		Nitro compound	NO_2	$\tilde{\nu}_{as}$(NO), $\tilde{\nu}_{s}$(NO)	
		trans-hoponitrite	*trans*-$N_2O_2^{2-}$	$\tilde{\nu}$(N = N)	

of the band at 1930 cm^{-1} first becomes stronger but then weakens as a function of increased temperature similar to the evolution of the $\tilde{\nu}_{lin}^{NCO}$(ceria). This suggests that the band at 1930 cm^{-1} reflects $\tilde{\nu}_{lin}^{NO}(Pt^{2+})$. Concerning CO ad-species, the peaks at 2129 and 2089 cm^{-1} are ascribed to $\tilde{\nu}_{lin}^{CO}(Pt^{2+})$ and $\tilde{\nu}_{lin}^{CO}(Pt^{\delta+})$ [10]. The $\tilde{\nu}_{lin}^{CO}(Pt^{2+})$ band initially grows when the temperature is increased and reaches maximum at 88 °C showing a red-shift of 4 cm^{-1}. It then gradually decreases with further increase of the temperature although it is clearly visible also at 208 °C. In contrast the $\tilde{\nu}_{lin}^{CO}(Pt^{\delta+})$ band is hardly visible above 185 °C. At the higher temperatures, the minor peak appearing at 2150 cm^{-1} can be assigned to CO linearly adsorbed on reduced ceria ($\tilde{\nu}_{lin}^{CO}(Ce^{3+})$). Moving to the region between 1000 and ca 1700 cm^{-1} many peaks are visible (cf. Table 1). The bands observed at 1605 and 1322 cm^{-1} at the lower temperatures are likely caused by weakly adsorbed NO_2. Both bands vanish quickly with increasing temperature. The bands at 1592, 1212 and 1010 cm^{-1} are related to bridged nitrates (br-NO_3) on ceria, whereas the bands at 1581, 1241 and 1033 cm^{-1} are bidentate nitrates (b-NO_3) on ceria. The band at 1434 cm^{-1} is more difficult to assign. It could originate from polydentate nitrate (p-NO_3) or, together with the band at 1322 cm^{-1}, water-solvated nitrate (NO_3(OH)). Another assignment is a nitro compound in which the nitrogen atom binds to ceria, but this seems to be less likely due to the presence of O_2. It could also be the asymmetric stretch of *trans*-hyponitrite but this is unlikely due to the lack of a band for the symmetric stretch $\tilde{\nu}_s$ expected at around 1100 cm^{-1}. The minor peak at 1474 cm^{-1} can be attributed to the asymmetric stretch of monodentate nitrite (m-NO_2), accompanied with the band at 1033 cm^{-1}. However, also polydentate carbonates (p-CO_3) are expected to cause a peak at this position. With increasing temperature, all these bands lose intensity. At 105 °C, some minor peaks assigned to carbonates appear and become clear at around 130 °C. The peak at 1434 cm^{-1} possibly originating from p-NO_3 at the start grows and blue-shifts and is therefore assigned to p-CO_3 at the elevated temperatures. The expected split band for a p-CO_3 species might be too weak to observe. Upon decreasing temperature (panel b), the CO oxidation reaction extinguishes as reflected by the continuous decrease of the intensity of the $\tilde{\nu}_{gas}^{CO_2}$ band. The intensity of the $\tilde{\nu}_{lin}^{CO}(Ce^{3+})$ band increases until 162 °C is reached, and then decreases and is hardly visible at 130 °C. Simultaneously, the intensity of the $\tilde{\nu}_{lin}^{NCO}$(ceria) band increases until 130 °C is reached. Upon further lowering of the temperature, the $\tilde{\nu}_{lin}^{NCO}$(ceria) band starts to diminish showing a blue-shift of around 6 cm^{-1} and a shoulder peak at around 2253 cm^{-1} that blue-shifts about 8 cm^{-1} becomes visible. The intensity of the $\tilde{\nu}_{lin}^{CO}(Pt^{2+})$ band at

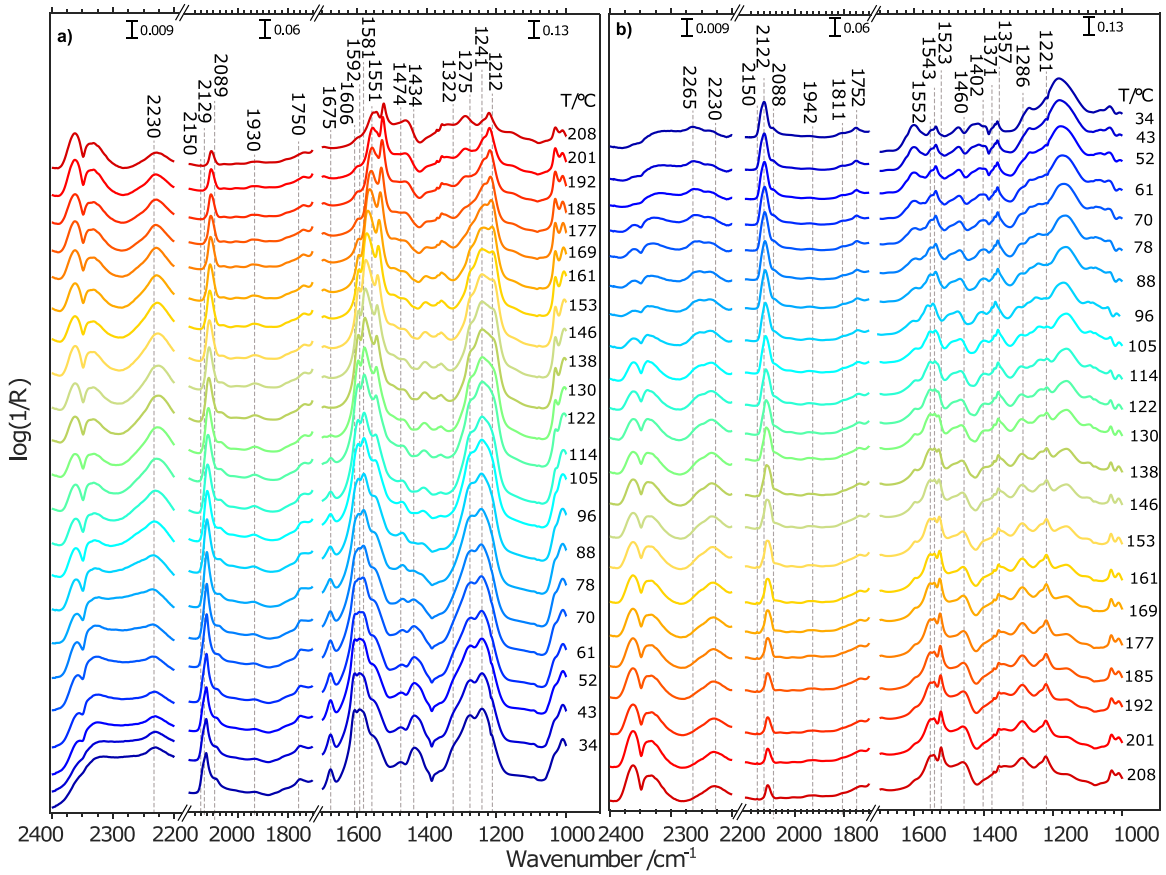

Fig. 4. Infrared difference spectra collected during CO oxidation in the presence of NO (0.2 vol% CO, 1 vol% O_2, 300 ppm NO and Ar as balance) over Pt/ceria while increasing (panels a) and decreasing (panels b) the sample temperature in steps between 34 and 209 °C.

2109 cm^{-1} gradually increases with a blue-shift of 13 cm^{-1} to 2122 cm^{-1}. The shoulder peak at 2086 cm^{-1} exhibits a blue-shift of around 30 cm^{-1}. The intensity of the $\tilde{\nu}_{lin}^{NO}(Pt^0)$ band may increase somewhat whereas the $\tilde{\nu}_{br}^{NO}(Pt^0)$ band is not visible even at the lowest temperature.

In summary, the evolution of IR bands in the 1000–1700 cm^{-1} region during CO oxidation ignition-extinction in the presence of NO clearly show that the adsorbate composition on the ceria surface changes from being occupied by nitrate species that upon increased temperature is replaced by carbonate species. These in turn (to some extent) decompose at the highest temperature. When lowering the temperature, carbonate species start to be replaced by nitrate species. Thus one can envisage that the NO inhibition is related to formation of nitrate species effectively hindering ceria lattice oxygen close to the rim of the platinum particles from taking part in the CO oxidation reaction at low temperatures as has been shown in previous works [3,4].

The corresponding results for the catalytic ignition-extinction of the CO oxidation over the Pt/alumina catalyst are shown in Fig. 5. The $\tilde{\nu}_{lin}^{CO}(Pt^{2+})$ band increases in intensity until 123 °C is reached from where it starts to decrease. At 131 °C, a $\tilde{\nu}_{gas}^{CO_2}$ band is visible, although it is very weak. A clear $\tilde{\nu}_{lin}^{NCO}$(alumina) band appears at around 88 °C and reaches its maximum intensity at 138 °C. Simultaneously, the $\tilde{\nu}_{lin}^{NO}(Pt^0)$ and $\tilde{\nu}_{br}^{NO}(Pt^0)$ bands disappear although some IR bands for nitrate species on the alumina are visible. The $\tilde{\nu}_{lin}^{NCO}$(alumina) is visible even at 209 °C. Upon decreasing the temperature, the intensity of the $\tilde{\nu}_{gas}^{CO_2}$ band remains until at 131 °C is reached where it suddenly drops in intensity and ceases with further decrease of the temperature. The intensity of the $\tilde{\nu}_{lin}^{NCO}$(alumina) band passes through a maximum during the cooling process. During the lowering of the temperature, the $\tilde{\nu}_{lin}^{CO}(Pt^{2+})$ band at 2109 cm^{-1} grows and the $\tilde{\nu}_{lin}^{CO}(Pt^{\delta+})$ band appears as a shoulder at 170 °C. When the final temperature is reached, a blue-shift of around 11 and 20 cm^{-1} is observed for the $\tilde{\nu}_{lin}^{CO}(Pt^{2+})$ and $\tilde{\nu}_{lin}^{CO}(Pt^{\delta+})$ band, respectively.

In essence, the evolution of IR bands in the 1000–1700 cm^{-1} region for the for the Pt/alumina catalyst during ignition-extinction is qualitatively similar to the case of Pt/ceria. At the lower temperatures, nitrate species dominate the alumina surface. When the temperature is increased and the CO oxidation starts (although to a minor extent), the alumina nitrates are slowly replaced with carbonates.

To deepen the discussion of the carbonate and nitrate formations, time-resolved infrared difference spectra collected during CO oxidation conditions in the presence of NO at 35 °C are shown in Fig. 6 for the Pt/ceria (panel a) and Pt/alumina (panel b). For the Pt/ceria, the two major IR bands at 2104 and 2090 cm^{-1} are assigned to $\tilde{\nu}_{lin}^{CO}(Pt^{2+})$ and $\tilde{\nu}_{lin}^{CO}(Pt^{\delta+})$. With increasing time, the $\tilde{\nu}_{lin}^{CO}(Pt^{2+})$ band blue-shifts by 25 cm^{-1} while also becoming more intense. At the start (t = 1 min), the peaks observed at 1606, 1393, 1218, 1037 cm^{-1} (and together with a peak at 3617 cm^{-1} not shown) can be ascribed to bridged hydrogen carbonate (br-(CO_2)OH). For this species, the bands at 1606 and 1393 cm^{-1} origins from splitting of the asymmetric stretch ($\tilde{\nu}_{as}$) of CO_3^{2-} whereas the band at 1037 cm^{-1} is the symmetric stretch ($\tilde{\nu}_s$). The bands at 1218 and 3617 cm^{-1} (not shown) signifies the OH bending (δ) and stretching ($\tilde{\nu}$) modes respectively [17,18]. At t = 30 min, a peak at 1186 cm^{-1} appears, which can be attributed to either a nitrosyl anion (NO^-) or the asymmetric stretch of a bidentate chelating nitrite, simply referred to as a bidentate nitrite (b-NO_2) as these species are spectroscopically indistinguishable [29]. The corresponding band for the

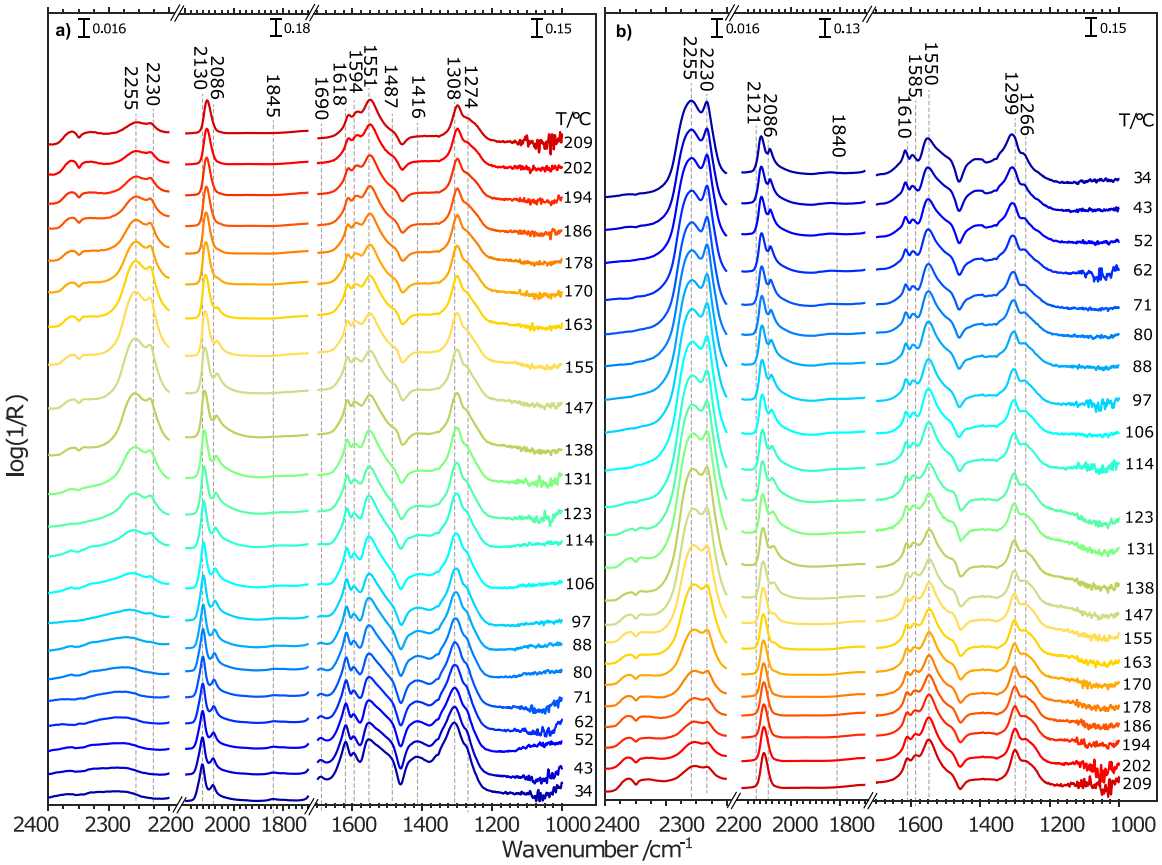

Fig. 5. Infrared difference spectra collected during CO oxidation in the presence of NO (0.2 vol% CO, 1 vol% O_2, 300 ppm NO and Ar as balance) over Pt/alumina while increasing (panels a) and decreasing (panels b) the sample temperature in steps between 34 and 209 °C.

symmetric stretch should appear in the region 1266–1314 cm^{-1} but may be difficult to observe due to overlapping with nitrate bands. Also, it can be somewhat masked by peaks from carbonate species (in the background spectrum) present as a result of the pretreatment. However, the combination band of $\widetilde{\nu}_{as}$ and $\widetilde{\nu}_{s}$ can be seen at 2477 cm^{-1} indicating the existence of b-NO_2. The two weak bands at 1361 and 1058 cm^{-1} can be ascribed to *cis*-hyponitrite (*cis*-$N_2O_2^{2-}$) on ceria. These bands disappear quickly and new peaks at 1605, 1591, 1581, 1551, 1475, 1433, 1322, 1276, 1240, 1212, 1033 and 1010 cm^{-1} grow, at the expense of a gradual decrease of the intensity of the band at 1186 cm^{-1}, and reach maximum intensity after two hours. Among these, the band at 1605 and 1322 cm^{-1} are likely caused by weakly adsorbed NO_2 as both bands disappear quickly when increasing temperature (cf. in Fig. 4a). The bands at 1591, 1212, and 1010 cm^{-1} are related to bridged nitrates (br-NO_3) on ceria, whereas the bands at 1581, 1240 and 1033 cm^{-1} are bidentate nitrates (b-NO_3) on ceria. The band at 1433 cm^{-1} is more difficult to assign. It could originate from polydentate nitrate (p-NO_3) or water-solvated nitrate (NO_3(OH)) together with the band at 1322 cm^{-1}. Another assignment is a nitro compound in which the nitrogen atom binds to ceria, which seems to be less likely due to the presence of O_2. A third assignment could be the asymmetric stretch of *trans*-hyponitrite but this is unlikely due to the lack of a band for the symmetric stretch $\widetilde{\nu}_{s}$ band at around 1100 cm^{-1}. The minor peak at 1475 cm^{-1} can be attributed to the asymmetric stretch of monodentate nitrite (m-NO_2), accompanied with the band at 1033 cm^{-1}. However, this peak could also be caused by polydentate carbonates (p-CO_3) as it remains upon increasing temperature and also blue-shifts. The expected split band might be too weak to observe. For Pt/alumina, two major IR bands at 2077 and 2090 cm^{-1} are seen, which are assigned to $\widetilde{\nu}_{lin}^{CO}(Pt^{\delta+})$. Upon increasing temperature, the $\widetilde{\nu}_{lin}^{CO}(Pt^{\delta+})$ bands shift to 2088 and 2130 cm^{-1}, which indicates the presence of $\widetilde{\nu}_{lin}^{CO}(Pt^{2+})$. At t = 5 min, the minor peaks at 1655 and 1228 cm^{-1} can be attributed to br-CO_3 or to bridged hydrogen carbonate (br-(CO_2)OH) considering the peak at 1429 cm^{-1}. At t = 40 min, nitrate species start to grow progressively for two hours on stream, where they reach maximum intensity. Another assignment might be NO_2 species on alumina. The broad peak observed at 1308 cm^{-1} might contain several species.

The time-resolved infrared spectra show that adding NO to the CO + O_2 feed results in nitrate ad-species inducing a clear oxidation of the platinum particles. In fact the build-up of nitrate species on both the ceria and alumina surfaces occurs faster in presence of both CO and NO as compared to NO exposure to CO pre-treated catalysts (cf. Figure S1). The $\widetilde{\nu}_{lin}^{CO}(Pt^{2+})$ bands blue-shifts by 25 cm^{-1} and an intensity transfer from low to high wavenumber is obvious. An increased platinum oxidation state by addition of NO to a CO + O_2 feed to Pt/alumina has previously been measured by X-ray absorption spectroscopy before [30]. Although NO can dissociate on Pt under net-reducing conditions, which would lead to the formation of O ad-species that may convert into PtO_x species [31,32], it is unlikely that this occurs under oxygen excess conditions. Rather, NO is oxidised to NO_2. The bands at 1605 and 1322 cm^{-1} are likely signifying weakly adsorbed NO_2, which disappear quickly when increasing the temperature (Fig. 5). As NO_2 is a strong oxidant one can speculate that it decomposes on some other Pt sites [33] leading to oxidation of the platinum particle. This, however, seems unlikely as it would involve oxidation and reduction of the same NO_x species, and the resulting O ad-species probably would react with CO and thus ignite the CO oxidation reaction. Instead, the spectroscopic data shows that NO/NO_2 form nitrate species on both Al_2O_3 and CeO_2, which may occur even without platinum [27,34]. Many of these species are likely formed close to or at the platinum-support boundary, thus

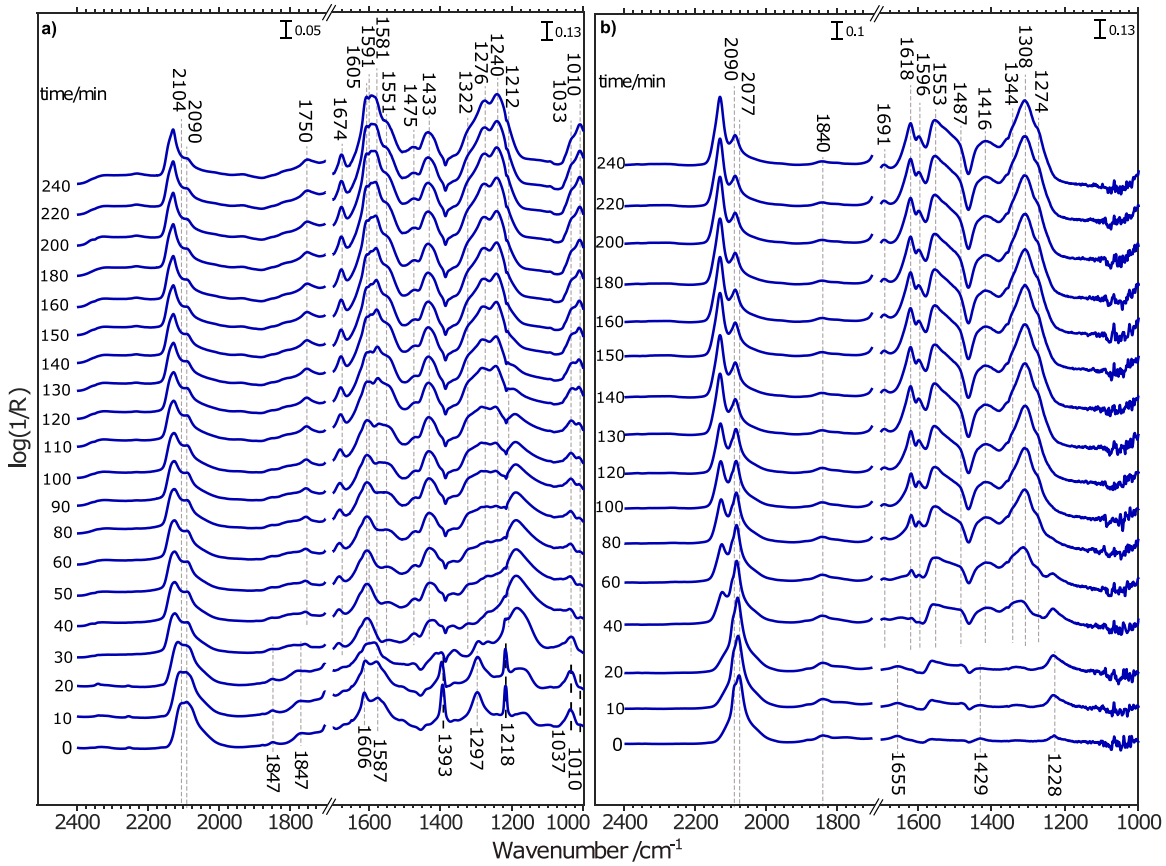

Fig. 6. Infrared difference spectra recorded while feeding 0.2 vol% CO, 1 vol% O_2 and 300 ppm NO (Ar as balance) at 35 °C over the Pt/ceria (panel a) and Pt/alumina (panel b) catalysts.

influencing the Pt particles. As nitrate species are likely to attract electrons, the Pt particles become oxidised. This interpretation goes hand in hand with that the Pt particles still can be covered by CO resulting in the clear $\tilde{\nu}_{lin}^{CO}(Pt^{2+})$ band.

The infrared spectroscopic results for ignition of the CO oxidation over NO pre-exposed catalysts are shown in Fig. 7. For Pt/ceria, again, $\tilde{\nu}_{lin}^{CO}(Pt^{2+})$ and $\tilde{\nu}_{lin}^{NO}(Pt^{0})$ bands are clearly seen. Also, IR bands for NO^{-} and b-CO_3 are seen at 34 °C. Upon increasing temperature, the $\tilde{\nu}_{gas}^{CO_2}$ band is visible from 69 °C while $\tilde{\nu}_{lin}^{CO}(Pt^{\delta+})$ and $\tilde{\nu}_{br}^{NO}(Pt^{0})$ bands as well as bands from br-CO_3 species are also visible. At 104 °C, the maximum intensity of the $\tilde{\nu}_{lin}^{CO}(Pt^{2+})$ band is seen and the $\tilde{\nu}_{lin}^{CO}(Pt^{2+})$ and $\tilde{\nu}_{lin}^{CO}(Pt^{\delta+})$ bands red-shifts by 9 and 5 cm^{-1}, respectively. Simultaneously, m-CO_3 becomes an evident species. For Pt/alumina, the IR bands for CO ad-species increase in intensity. Clear red-shifts can be seen for the $\tilde{\nu}_{lin}^{CO}(Pt^{2+})$ and $\tilde{\nu}_{lin}^{CO}(Pt^{\delta+})$ bands by 5 and 14 cm^{-1}, respectively. Also, their intensities passes a maximum at 132 °C. Reaching 140 °C, an abrupt change in intensity of the $\tilde{\nu}_{lin}^{CO}(Pt^{\delta+})$ band is observed.

The formation of nitrates at the platinum-support boundary can explain the NO inhibition effect for Pt/ceria and Pt/alumina. For Pt/ceria it is suggested to block ceria lattice oxygen to participate in the reaction, thus quenching the Mars-van Krevelen mechanism responsible for the low-temperature activity. For Pt/alumina, the NO inhibition effect on the ignition is very similar for co-feeding and pre-adsorption of NO. In this case nitrate formation affects the oxidation state of the platinum, which is suggested to be most significant for platinum atoms at the rim of the particles. Thus these sites become electron deficient and likely less active for CO oxidation such that ignition occurs once the CO desorption becomes significant.

4. Conclusions

The presence of NO shifts the CO conversion, both ignition and extinction profiles, over alumina and ceria supported platinum to higher temperatures. Pre-adsorption of NO also shifts the ignition profiles to higher temperatures, although the slope of the CO conversion curve once light-off takes place is similar to the case without pre-adsorbed NO. It is thus clear that NO suppresses the low-temperature CO oxidation over both types of catalysts. For Pt/ceria, a similar shift has been seen upon adding NO_2 to catalytic systems with larger Pt particles, although not to this extent [2]. In case of the Pt/ceria catalyst, spectroscopic data indicates that NO inhibits the Mars-van Krevelen mechanism operating at low temperatures. For temperatures at and close (above) the light-off temperature, for which the CO self-poisoning is expected to be minor, the CO conversion may suffer from competitive adsorption of CO and NO on free Pt sites. The less steep slope of the CO oxidation ignition profile for continuous feed of NO as compared to that of pre-adsorbed NO supports this. The formation of nitrates at low temperatures seem to induce a clear oxidation of a significant number of the Pt sites, as reflected by the vibration frequencies of adsorbed CO species, likely leading to that these sites become less active for CO oxidation.

CRediT authorship contribution statement

Mengqiao Di: Investigation, Methodology, Formal analysis, Writing Ű Original Draft. **Andreas Schaefer**: Supervision, Writing Ű Review & Editing. **Felix Hemmingsson**: Investigation, Visualization. **Tamsin Bell**: Resources. **Yanyue Feng**: Investigation. **Magnus Skoglundh**: Funding acquisition, Supervision. **David Thompsett**: Resources, Conceptualization. **Per-Anders Carlsson**: Conceptualization, Writing Ű Review & Editing, Supervision, Project administration, Funding

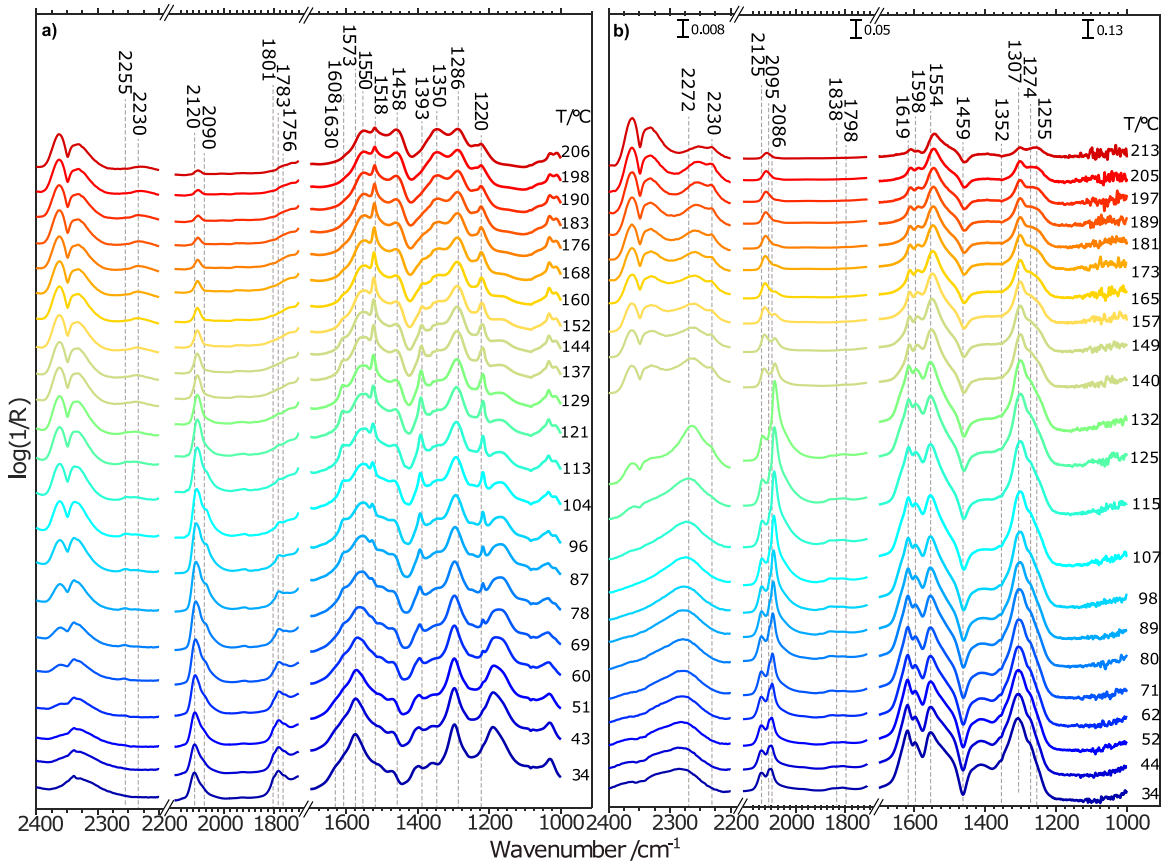

Fig. 7. Infrared difference spectra recorded after pre-adsorption of NO followed by catalytic CO oxidation ignition for Pt/ceria (panel a) and Pt/alumina (panel b). CO_2 gas phase spectra with noted CO conversions measured with mass spectrometry and spectral region for CO adsorbed on Pt and carbonates/nitrates with noted sample temperatures in °C in presence of 0.2 vol% CO and 1 vol% O_2.

acquisition.

Declaration of Competing Interest

The authors declare that they have no known competing financial interests or personal relationships that could have appeared to influence the work reported in this paper.

Data Availability

The authors are unable or have chosen not to specify which data has been used.

Acknowledgements

The authors thank the Swedish Research Council through the projects -IJSynergistic Development of X-ray Techniques and Applicable Thin Oxides for Sustainable Chemistry-İ (Dnr. 2017-06709) and "Infrared Spectroscopy in Time and Space" (Dnr. 2019-05528). Parts of this research were carried out at the Chalmers Materials Analysis Laboratory (CMAL) and we thank Stefan Gustafsson and Ludvig de Knoop for assistance. The work was carried out within the Competence Centre for Catalysis, which is hosted by Chalmers University of Technology and financially supported by the Swedish Energy Agency (52689-1) and the member companies AB Volvo, ECAPS AB, Johnson Matthey AB, Preem AB, Scania CV AB, Umicore Denmark ApS, and Volvo Car Corporation AB.

Appendix A. Supporting information

Supplementary data associated with this article can be found in the online version at doi:10.1016/j.cattod.2023.114394.

References

[1] S. Fouladvand, M. Skoglundh, P.-A. Carlsson, A transient in situ infrared spectroscopy study on methane oxidation over supported Pt catalysts, Catal. Sci. Technol. 4 (2014) 3463–3473.
[2] P.A. Carlsson, M. Skoglundh, Low-temperature oxidation of carbon monoxide and methane over alumina and ceria supported platinum catalysts, Appl. Catal. B: Environ. 101 (2011) 669–675.
[3] M. Di, K. Simmance, A. Schaefer, Y. Feng, F. Hemmingsson, M. Skoglundh, T. Bell, D. Thompsett, L.I. Ajakaiye Jensen, S. Blomberg, P.A. Carlsson, Chasing PtO_x species in ceria supported platinum during CO oxidation extinction with correlative operando spectroscopic techniques, J. Catal. 409 (2022) 1–11.
[4] N. Bosio, M. Di, M. Skoglundh, P.-A. Carlsson, H. Grönbeck, Interface reactions dominate low-temperature CO oxidation activity over Pt/CeO_2, J. Phys. Chem. C 126 (2022) 16164–16171.
[5] Rasband WS.ImageJ, 2021 -06–04.⟨https://imagej.nih.gov/ij/⟩.
[6] C. Zhang, J. Gustafson, L.R. Merte, J. Evertsson, K. Norén, S. Carlson, H. Svensson, P.-A. Carlsson, An in situ sample environment reaction cell for spatially resolved X-ray absorption spectroscopy studies of powders and small structured reactors, Rev. Sci. Instrum. 86 (2015), 033112.
[7] P.-A. Carlsson, P. Thormählen, M. Skoglundh, H. Persson, E. Fridell, E. Jobson, B. Andersson, Periodic control for improved low-temperature catalytic activity, Top. Catal. 16 (2001) 343–347.
[8] P.-A. Carlsson, M. Skoglundh, E. Fridell, E. Jobson, B. Andersson, Induced low temperature catalytic ignition by transient changes in the gas composition, Catal. Today 73 (2002) 307–313.
[9] P.-A. Carlsson, M. Skoglundh, P. Thormählen, B. Andersson, Low-temperature, CO oxidation over a Pt/Al_2O_3 monolith catalyst investigated by step-response experiments and simulations, Top. Catal. 30 (2004) 375–381.
[10] P.-A. Carlsson, L. Österlund, P. Thormählen, A. Palmqvist, E. Fridell, J. Jansson, M. Skoglundh, A transient in situ FTIR and XANES study of CO oxidation over Pt/Al_2O_3 catalysts, J. Catal. 226 (2004) 422–434.

[11] Z.M. El-Bahy, Adsorption of CO and NO on ceria- and Pt-supported TiO_2: In situ FTIR study, Mod. Res. Catal. 02 (2013) 136–147.
[12] E.C. Adams, M. Skoglundh, P. Gabrielsson, P.-A. Carlsson, Passive scr: the effect of h 2 to no ratio on the formation of nh 3 over alumina supported platinum and palladium catalysts, Top. Catal. 59 (2016) 970–975.
[13] P. Bazin, O. Saur, J.C. Lavalley, M. Daturi, G. Blanchard, FT-IR study of CO adsorption on Pt/CeO_2: characterisation and structural rearrangement of small Pt particles, Phys. Chem. Chem. Phys. 7 (2005) 187–194.
[14] E. Ivanova, M. Mihaylov, F. Thibault-Starzyk, M. Daturi, K. Hadjiivanov, FTIR spectroscopy study of CO and NO adsorption and co-adsorption on Pt/TiO_2, J. Mol. Catal. A: Chem. 274 (2007) 179–184.
[15] F. Hemmingsson, A. Schaefer, M. Skoglundh, P.A. Carlsson, CO_2 methanation over Rh/CeO_2 studied with infrared modulation excitation spectroscopy and phase sensitive detection, Catalysts 10 (2020).
[16] C. Li, Y. Sakata, T. Arai, K. Domen, K.I. Maruya, T. Onishi, Carbon monoxide and carbon dioxide adsorption on cerium oxide studied by Fourier-transform infrared spectroscopy. Part 1. - Formation of carbonate species on dehydroxylated CeO_2, at room temperature, J. Chem. Soc. Faraday Trans. 1: Phys. Chem. Condens. Phases 85 (1989) 929–943.
[17] C. Binet, M. Daturi, J.C. Lavalley, IR study of polycrystalline ceria properties in oxidised and reduced states, Catal. Today 50 (1999) 207–225.
[18] G.N. Vayssilov, M. Mihaylov, P.S. Petkov, K.I. Hadjiivanov, K.M. Neyman, Reassignment of the vibrational spectra of carbonates, formates, and related surface species on ceria: a combined density functional and infrared spectroscopy investigation, J. Phys. Chem. C 115 (2011) 23435–23454.
[19] M.Y. Mihaylov, V.R. Zdravkova, E.Z. Ivanova, H.A. Aleksandrov, P.S. Petkov, G. N. Vayssilov, K.I. Hadjiivanov, Infrared spectra of surface nitrates: revision of the current opinions based on the case study of ceria, J. Catal. 394 (2021) 245–258.
[20] K.I. Hadjiivanov, Identification of neutral and charged N_xO_y surface species by IR spectroscopy, Catal. Rev. - Sci. Eng. 42 (2000) 71–144.
[21] L. Zhang, J. Pierce, V.L. Leung, D. Wang, W.S. Epling, Characterization of ceria's interaction with NO_x and NH_3, J. Phys. Chem. C 117 (2013) 8282–8289.
[22] G. Qi, R.T. Yang, R. Chang, MnO_x-CeO_2 mixed oxides prepared by co-precipitation for selective catalytic reduction of NO with NH3 at low temperatures, Appl. Catal. B: Environ. 51 (2004) 93–106.
[23] M.Y. Mihaylov, E.Z. Ivanova, H.A. Aleksandrov, P.S. Petkov, G.N. Vayssilov, K. I. Hadjiivanov, Species formed during NO adsorption and NO + O_2 co-adsorption on ceria: a combined FTIR and DFT study, Mol. Catal. 451 (2018) 114–124.
[24] M.Y. Mihaylov, E.Z. Ivanova, G.N. Vayssilov, K.I. Hadjiivanov, Revisiting ceria-NO_x interaction: FTIR studies, Catal. Today 357 (2020) 613–620.
[25] H. Du, C.T. Williams, A.D. Ebner, J.A. Ritter, In situ FTIR spectroscopic analysis of carbonate transformations during adsorption and desorption of CO_2 in K-promoted HTlc, Chem. Mater. 22 (2010) 3519–3526.
[26] T.J. Toops, D.B. Smith, W.S. Epling, J.E. Parks, W.P. Partridge, Quantified NO_x adsorption on Pt/K/gamma-Al_2O_3 and the effects of CO_2 and H_2O, Appl. Catal. B: Environ. 58 (2005) 255–264.
[27] B. Westerberg, E. Fridell, A transient FTIR study of species formed during NO_x storage in the Pt/BaO/Al − $2O_3$ system, J. Mol. Catal. A: Chem. 165 (2001) 249–263.
[28] A. Zecchina, Infrared spectroscopy of adsorbed species on the surface of transition metal oxides, Spectrochim. Acta Part A: Mol. Spectrosc. 47 (1991) 823–824.
[29] M.Y. Mihaylov, E.Z. Ivanova, G.N. Vayssilov, K.I. Hadjiivanov, Revisiting ceria-NO_x interaction: FTIR studies, Catal. Today 357 (2020) 613–620.
[30] A.M. Gänzler, M. Casapu, F. Maurer, H. Störmer, D. Gerthsen, G. Ferré, P. Vernoux, B. Bornmann, R. Frahm, V. Murzin, M. Nachtegaal, M. Votsmeier, J.-D. Grunwaldt, Tuning the Pt/CeO_2 interface by in situ variation of the Pt particle size, ACS Catal. 8 (2018) 4800–4811.
[31] Q. Ge, M. Neurock, Structure dependence of NO adsorption and dissociation on platinum surfaces, J. Am. Chem. Soc. 126 (2004) 1551–1559.
[32] M.A. Van Spronsen, J.W. Frenken, I.M. Groot, Observing the oxidation of platinum, 2017 8:1, Nat. Commun. 8 (2017) 1–7.
[33] B.A. Morrow, R.A. McFarlane, L.E. Moran, Infrared study of the reaction between NO and 0_2 and of the adsorption of $N0_2$ on platinum, Masel. R. I.; Stolt, K. Surf. Sci. 89 (1985) 3052.
[34] A. Filtschew, C. Hess, Unravelling the mechanism of no and no2 storage in ceria: The role of defects and ce-o surface sites, Appl. Catal. B: Environ. 237 (2018) 1066–1081.